Astron. Astrophys. 275, 433–450 (1993)

ASTRONOMY AND ASTROPHYSICS

Statistical properties of stellar populations and surface-brightness fluctuations in galaxies

A. Buzzoni

Osservatorio Astronomico di Brera, Via Brera, 28, I-20121 Milano, Italy

Received August 24, 1992; accepted January 28, 1993

Abstract. Some relevant concepts dealing with the statistical properties of stellar populations are approached and explored in detail defining the effective stellar contributors $N_{\rm eff}$, and the effective luminosity $l_{\rm eff}$ of a stellar aggregate. These two quantities strictly relate to the distinctive properties of a stellar population, and basically modulate the intrinsic statistical scatter in a pixel-to-pixel surface photometry of a galaxy (providing that photon scatter and other perturbing effects are excluded).

The effective luminosity and number contributors in simple stellar populations have been calculated through a set of 206 models based on Buzzoni's (1989) code for population synthesis, including also the case of composite stellar populations.

The results have been applied to the Tonry–Schneider (1988) method on galaxy surface-brightness fluctuations deriving new distances for M 32 and galaxies in the Virgo cluster as well as in the Leo, Fornax, and Eridanus groups observed by Tonry and colleagues. The distance of Virgo is found to be 15.3 Mpc supporting Tonry's (1991) previous estimate.

Also the distance of the Galactic globular cluster M 3 has been derived resting on the complete sample of 10 000 stars by Buonanno et al. (1986, 1988). We obtain a distance modulus $(m-M)_0=15.01\pm0.13$ in excellent agreement with other current estimates confirming the reliability of the Tonry–Schneider method once accurate theoretical models for population systhesis are considered.

Key words: galaxy: globular clusters: M 3 – galaxies: distances and redshifts – galaxies: photometry – evolution

1. Introduction

A study of integral statistical properties of stellar populations in galaxies is of great interest in order to achieve a realistic description of galactic properties. Stars provide virtually all the light in a normal galaxy tracing its morphology and modulating its color.

It is clear however that such a contribution does not come from a continuous texture but rather from a set of point sources, subject to Poissonian statistics in their number counts. As a consequence, even considering integrated properties of homogeneous stellar samples in a galaxy we should expect apparent fluctuations induced by statistics.

Due to its nature, the relative size of such statistical fluctuations decreases as $1/\sqrt{N}$ with increasing the total number N of stars contained in a given sample. In a typical galaxy at the distance of the Virgo cluster, for example, we expect a surface density of about 10^6 stars arcsec^{-2}. When observing with a 0.3″ pxl^{-1} detector we would collect light from about 10^5 stars per resolution element with a relative pixel-to-pixel scatter of $\pm0.3\%$. This scattering is increased by photon statistics while the diffraction figure of the telescope and the atmospheric seeing contributes in blurring the image and smoothing the mottling on galactic surface.

As well known, such severe crowding conditions prevent us from resolving details of single stars on the surface of external galaxies, with the only partial exception of M 31 and a few other galaxies in the Local Group. Also space observations, albeit improving, would hardly disentangle the problem that would be limited in any case by instrumental diffraction. One main consequence is that any distance calibrator resting on normal stars cannot be longer effective beyond the Local Group.

A better knowledge of statistics in stellar populations would help however in this regard. Stars with different temperature contribute in different ways at a given photometric passband. For example, when observing in the infrared an aggregate of blue stars one could be sure to easily pierce the cluster as virtually no star would be detected. Therefore, from the purely observational point of view the crowding on galaxy surface (even disregarding any physical effect of gas and dust) depends on wavelength. Since we would be looking at different number of effective stellar contributors in every wavelength (Buzzoni 1988), this concept is basically related to the problem of the statistical fluctuations in the galactic surface brightness.

This phenomenon has been used as an ingenious and powerful tool to determine extragalactic distances. The main asset of this idea, first theorized by Tonry & Schneider (1988), is that we can derive quite accurately

the mean stellar luminosity in galaxies considering the stellar population as a whole and avoiding thus to resolve any single star. From the observational point of view this is of great advantage allowing to achieve high performances also from ground-based telescopes.

In order to apply this technique with confidence it is mandatory to consistently compare observations with theoretical reference models for stellar populations. Indeed, as discussed in Tonry et al. (1990) any uncertainty in this match would result in a large error on the inferred distances.

In this work we intend to go in depth into different questions dealing with the statistical behaviour of stellar populations in galaxies. Special care will be devoted in particular to the problem of the crowding in galaxy surface photometry as a result of effective stellar contributors, and to a possible application of our results to the Tonry–Schneider method on surface-brightness fluctuations. Although we will especially focus our analysis on elliptical galaxies, we will demonstrate that our conclusions might be fully applicable in the proper context of the study of the Galactic globular clusters as well.

In Sect. 2 we discuss some theoretical aspects on population statistics, developing a set of 206 reference models for stellar populations in Sect. 3. The Tonry–Schneider method will be more extensively approached in Sect. 4 on the basis of our new results. The relevant conclusions are finally summarized in Sect. 5.

2. Theoretical framework

2.1. *Effective contributors in a stellar population*

It could be useful to summarize here some simple but fundamental concepts governing statistics in stellar populations. A similar approach to the question has been developed independently by Tonry & Schneider (1988) and Buzzoni (1988, 1989) leading to two different but equivalent definitions of the problem. It is worth then to unify here both approaches.

Due to its Poissonian nature, the mean and variance in the number counts of a sample of just one star is of course 1 ± 1. If a sample of N stars, all of the same luminosity l is considered, the total luminosity will be $L_{\rm TOT} = \sum_N l$ while its standard devaition will be $\sigma_{L_{(\rm TOT)}} = (\sum_N l^2)^{1/2}$. Hence the amplitude of expected fluctuations in an unresolved sample would be:

$$\frac{\sigma_{L_{(\rm TOT)}}}{L_{\rm TOT}} = \frac{\sqrt{N}l}{Nl} = 1/\sqrt{N}. \quad (1)$$

When considering the total light from a stellar population, although every star contributes at any wavelength to the total luminosity, one could imagine that due to its different luminosity and colors, its relative weight within the population depends on wavelength. As discussed in Buzzoni (1988, 1989), in the more general case we are dealing with a sample of stars of different luminosities, Eq. (1) remains valid as a descriptor of the fluctuations as long as we define the right-hand side term as $1/\sqrt{N_{\rm eff}}$. The quantity $N_{\rm eff}$ should be regarded therefore as an "effective" number of contributors at a given wavelength. Of course, its meaning is purely statistical, and not related to star counts in a deterministic way. We always have the condition that $N_{\rm eff} \leq N$, and in addition $N_{\rm eff}$ is a function of λ. Once this function is known for a given total reference luminosity it can be calculated for any other value as it scales linearly with $L_{\rm TOT}$. We could also conclude that the ratio $S = N_{\rm eff}/N$ is a measure of the statistical entropy of the population at a given λ: the more homogeneously $L_{\rm TOT}$ is shared by stars the larger and closer to unity will be S.

The exact knowledge of $N_{\rm eff}$ as a function of wavelength is useful to calculate the expected pixel-to-pixel fluctuation in the apparent integrated colors for an aggregate of stars. In general, the first term of equivalence in Eq. (1) gives also the scatter in magnitude of the total luminosity at a given wavelength so that $\sigma(\rm mag) = 1/\sqrt{N_{\rm eff}}$. Therefore, considering for example the color $B-V$ we have

$$\sigma_{B-V} = |\sigma_B - \sigma_V|. \quad (2)$$

This relation comes from the general equation

$$\sigma^2_{X-Y} = \sigma^2_X + \sigma^2_Y - 2\rho\sigma_{(X,Y)}, \quad (3)$$

where as usual $\sigma_{(X,Y)}$ is the covariance of the statistical variables X and Y. Since the correlation coefficient linking the statistical populations in the V band and that in B is $\rho = 1$ (because although with different weight the same stars contribute both to the flux in V and B) it must hold that $\sigma_{X,Y} = \sigma_X \sigma_Y$ and Eq. (2) directly stems with little arithmetic.

It is worth stressing that the correct evaluation of color variance related to number-count statistical fluctuations does not derive from simple sum of variances in the two single bands (as usually made for photometric errors and erroneously adopted also in Buzzoni 1989). In such case, we will roughly overestimate the true value.

Applying our results to the previous example of a typical galaxy in the Virgo cluster, for which we would sample about $10^5 L_\odot$ pxl^{-1}, an appropriate estimate of the effective contributors (see Fig. 1) would predict $N_{\rm eff} \sim 7000$ in B, and 3000 in V getting thus $\sigma(B-V) = 0.006$. Including the near-infrared I band (and assuming the same CCD scale per pixel) only 500 effective contributors are expected so that we would obtain $\sigma(V-I) = 0.03$. In both cases it is fair to conclude that the accurate observations maximizing photon statistics would certainly be able to detect such an intrinsic color fluctuation from pixel-to-pixel even for such distant galaxies (the scatter in color is distance independent).

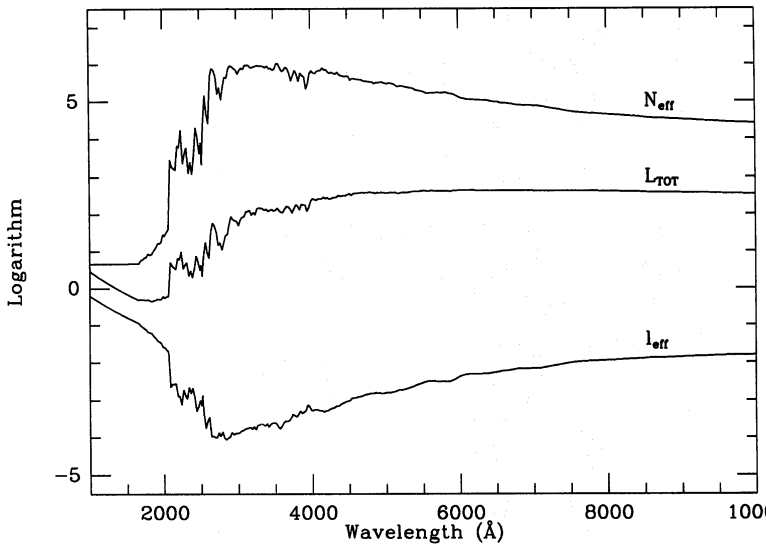

Fig. 1. Logarithm of effective luminosity ($l_{\rm eff}$) and number contributors ($N_{\rm eff}$) for a 15 Gyr simple stellar population of solar metallicity with Salpeter IMF. A direct relationship links $l_{\rm eff}$ and $N_{\rm eff}$ with the total luminosity of the population ($L_{\rm TOT}$) also displayed: i.e. $L_{\rm TOT}=l_{\rm eff}\times N_{\rm eff}$. Data have been normalized to a total bolometric luminosity of $10^7 L_\odot$

2.2. *Effective luminosity and distance determination*

Following Tonry & Schneider (1988), let us consider the ratio of the expected variance of a stellar population to its total luminosity:

$$\frac{\sigma^2_{L(\rm TOT)}}{L_{\rm TOT}}=\frac{\sum_N l^2}{\sum_N l}=l_{\rm eff}. \tag{4}$$

This ratio can be interpreted as a mean luminosity of the stars in a population obtained using the stellar luminosity itself as a weighting factor. If every star has the same luminosity then $l_{\rm eff}=L_{\rm TOT}/N$, otherwise $l_{\rm eff}\geq L_{\rm TOT}/N$. There is a direct link between Eq. (2) and Eq. (4) as it is apparent also in Fig. 1. In fact, the relation

$$\log N_{\rm eff}+\log l_{\rm eff}=\log L_{\rm TOT}, \tag{5}$$

simply states that the effective luminosity $l_{\rm eff}$ and number $N_{\rm eff}$ are those corresponding to a maximum entropy population providing $L_{\rm TOT}$. This also means that both quantities are fully equivalent statistical descriptors to mark a stellar population. This fact explains therefore the complementarity of the approach of Tonry & Schneider (1988) and Buzzoni (1988, 1989).

In practice, both $N_{\rm eff}$ or $l_{\rm eff}$ can be useful distance estimators through Eqs. (1) or (4). Following Tonry & Schneider (1988), and scaling Eq. (4) to apparent fluxes we can write

$$\frac{\sigma^2_{f(\rm TOT)}}{f_{\rm TOT}}=\frac{1}{4\pi D^2}\frac{\sigma^2_{L(\rm TOT)}}{L_{\rm TOT}}=\frac{l_{\rm eff}}{4\pi D^2}, \tag{6}$$

where $f_{\rm TOT}$ is the integrated flux observed at a given photometric passband. Once an appropriate value of $l_{\rm eff}$ can be assumed from a study of the integrated properties of the galactic stellar population, the distance D can be obtained from equation. Contrary to the conclusion of Tonry et al. (1990), the effectiveness of the method is not affected by the possible dependence of $l_{\rm eff}$ on the distinctive parameters of the stellar population. In any case, what counts eventually is a proper theoretical calibration via reference models for population synthesis. A combined observational approach resting on multicolor photometry would certainly be able to indicate the relevant range of models consistent with the observational data.

2.3. *Crowding*

The concept of effective contributors in a stellar population can help considering more quantitatively the effect of crowding in galactic surface photometry. As well known, what really limits the resolution of external galaxies into stars is not only the high density of objects but rather the atmospheric seeing effects that merge the otherwise point sources. This is why the only successful attempts to see stars have been achieved under superb seeing conditions and with the new-generation telescopes (cf. for example the excellent works by Mould et al. 1983, 1984 on NGC 147 and NGC 205; Freedman 1988, 1989 on IC 1613 and M 32; Wilson et al. 1990 on M 33). Yet, galaxies beyond the Local Group cannot be resolved with present technological capabilities.

The possibility of seeing deep in (or even through) an aggregate of stars strongly depends on the number of luminous stellar sources per unit area. As previously discussed, from the observational point of view a stellar aggregate does not appear with the same density at the different wavelengths. Turning again to our Virgo galaxy, if we observe under 1″ FWHM seeing, the apparent area of one star would take about 5 arcsec^2 (at a 3-σ radius). This means that with our assumed scale we would be able to discriminate reasonably well single stars in the galaxy if we have in average $N_{\rm eff}=0.02$ bright objects/pixel. Under our sampling conditions, and looking at Fig. 1, this requirement might be fulfilled only observing in the extreme ultraviolet shortward of 2000 Å.

As an instructive example we can also consider the case of a typical $10^5 L_\odot$. Galactic globular cluster comparing

with the recent ultraviolet observations of M 79 obtained with UIT (Hill et al. 1992). Suppose the cluster has a population of blue horizontal branch (HB) stars, as the case for M 79, we predict at 1520 Å about one effective stellar contributor per $1000 L_{\odot}$ sampled (in bolometric). This means that ultraviolet luminous stars should be so sparse that we can pick them up even in the core of the cluster, that would appear therefore nearly transparent (see Fig. 1 in Hill et al. 1992). Crowding conditions dramatically worsen moving to slightly longer wavelengths, and yet the core of the clusters cannot be resolved anymore imaging at 2000 Å (Laget et al. 1992).

To summarize, we can conclude that the distance limit (D) at which we might still perform good stellar photometry in a distant galaxy simply depends on the seeing FWHM and on the apparent stellar density (related to the total number of effective contributors) as $D \times \mathrm{FWHM} \propto 1/\sqrt{N_{\mathrm{eff}}}$. This means for example that in order to achieve for M 32 a performance in V-photometry comparable to that obtained by Freedman (1989) observing in I and with a 0.6″ FWHM we would need a factor of three better seeing conditions. It is quite evident therefore how discouraging are observational constraints when attempting to resolve at optical wavelengths stars in external galaxies.

3. Reference models for population synthesis

3.1. Simple stellar populations

Based on Buzzoni's (1989) code for population synthesis a grid of 186 models was computed for simple stellar populations (SSPs) exploring in detail the relevant quantities involved in our previous discussion. Results are reported in Tables 1–3.

Table 1a. SSP models for $s = 1.35$ ($\eta = 0.3$)

Log Z	[Fe/H]	Age (Gyr)	$\overline{V}$	$\overline{U}-\overline{V}$	$\overline{B}-\overline{V}$	$\overline{V}-\overline{R}$	$\overline{V}-\overline{I}$	$\overline{V}-\overline{J}$	$\overline{V}-\overline{K}$
−4.00	−2.27	8.0	−2.65	0.10	0.61	0.62	1.03	1.37	3.36
		10.0	−1.76	1.58	1.12	0.95	1.61	2.23	3.33
		12.5	−1.18	2.14	1.35	1.12	1.89	2.64	3.71
		15.0	−0.94	2.20	1.37	1.13	1.90	2.66	3.73
		18.0	−0.74	2.18	1.36	1.12	1.89	2.64	3.70
−3.00	−1.27	8.0	−0.85	3.08	1.77	1.43	2.42	3.35	4.58
		10.0	−0.63	3.05	1.76	1.44	2.44	3.37	4.61
		12.5	−0.44	2.96	1.72	1.41	2.40	3.32	4.54
		15.0	−0.34	2.89	1.69	1.39	2.36	3.27	4.47
		18.0	−0.22	2.80	1.66	1.37	2.33	3.22	4.41
−2.00	−0.25	4.0	0.08	3.37	2.12	1.99	3.42	4.65	6.19
		5.0	0.21	3.37	2.10	1.96	3.38	4.60	6.14
		6.0	0.35	3.33	2.08	1.96	3.38	4.60	6.14
		8.0	0.54	3.25	2.04	1.94	3.35	4.57	6.10
		10.0	0.73	3.13	1.99	1.93	3.34	4.56	6.10
		12.5	0.89	2.98	1.93	1.90	3.30	4.50	6.03
		15.0	1.05	2.73	1.83	1.87	3.28	4.48	6.02
−1.77	−0.02	4.0	0.40	3.32	2.17	2.15	3.67	4.96	6.57
		5.0	0.57	3.29	2.15	2.15	3.68	4.98	6.61
		6.0	0.72	3.24	2.12	2.13	3.67	4.97	6.60
		8.0	0.94	3.14	2.06	2.11	3.64	4.94	6.57
		10.0	1.09	3.04	2.01	2.09	3.62	4.91	6.55
		12.5	1.28	2.84	1.91	2.06	3.59	4.89	6.53
		15.0	1.41	2.58	1.80	2.02	3.55	4.85	6.50
−1.54	0.22	4.0	0.86	3.10	2.13	2.29	3.94	5.32	7.04
		5.0	1.00	3.07	2.11	2.29	3.95	5.34	7.08
		6.0	1.16	3.02	2.07	2.27	3.93	5.32	7.06
		8.0	1.39	2.88	1.98	2.24	3.91	5.32	7.08
		10.0	1.53	2.78	1.91	2.21	3.87	5.28	7.05
		12.5	1.69	2.60	1.81	2.16	3.82	5.22	6.99
		15.0	1.83	2.30	1.66	2.10	3.76	5.18	6.96

In these tables we list the effective absolute magnitude $\bar{V}$ from Eq. (4), and the derived effective colors $\bar{U}-\bar{V}$, $\bar{B}-\bar{V}$, $\bar{V}-\bar{R}$, $\bar{V}-\bar{I}$, $\bar{V}-\bar{J}$, $\bar{V}-\bar{K}$ in the Johnson system. Models are displayed assuming three different values for the IMF power-law index ($s=1.35$, 2.35, and 3.35 with the Salpeter value equal to 2.35), and two choices of the mass loss coefficient $\eta=0.3$ and 0.5 in the Reimers' (1975) notation. A red clump (R-HB; cf. Buzzoni 1989) for the HB morphology is assumed throughout.

Supplementary information for models in Table 2a are given in Table 4 where we report both the total number of (luminous) stars ($N_{\rm TOT}$), and the effective stellar contributors $N_{\rm eff}$ per unit bolometric solar luminosity at the different bands. From these data one immediately derives that the entropy coefficient S smoothly decreases from about 10^{-2} in U to 10^{-4} in the K band.

A further set of 20 models, more appropriate for fitting globular clusters, has been added and reported in Table 5. Here we explore the influence of different HB morphologies on the effective magnitudes and colors of the SSPs. An intermediate (I-HB) and blue (B-HB) morphology are attributed to 15 Gyr models following the evolution at the different ages according to Buzzoni's (1989) prescriptions.

As shown in Fig. 2, a striking difference emerges between effective colors of SSPs and their integrated colors (cf. Table 5 in Buzzoni 1989). For example, a 15 Gyr Salpeter population of solar metallicity yields $\bar{B}-\bar{V}=1.79$ while $B-V=0.93$. This can be understood from Eq. (5) that implies $(N^B_{\rm eff}\,l^B_{\rm eff}/N^V_{\rm eff}\,l^V_{\rm eff})=(L^B_{\rm TOT}/L^V_{\rm TOT})$. As a general rule, the difference in the number of effective stellar contributors to the two photometric bands reflects on a difference in the effective colors respect to the integrated ones.

Table 1b. SSP models for $s=1.35$ ($\eta=0.5$)

Log Z	[Fe/H]	Age (Gyr)	$\bar{V}$	$\bar{U}-\bar{V}$	$\bar{B}-\bar{V}$	$\bar{V}-\bar{R}$	$\bar{V}-\bar{I}$	$\bar{V}-\bar{J}$	$\bar{V}-\bar{K}$
−4.00	−2.27	8.0	−2.26	0.28	0.63	0.63	1.06	1.42	3.22
		10.0	−1.47	1.38	1.02	0.88	1.49	2.05	3.16
		12.5	−0.89	1.92	1.25	1.04	1.76	2.45	3.48
		15.0	−0.67	2.01	1.28	1.06	1.79	2.50	3.51
		18.0	−0.45	1.98	1.26	1.05	1.79	2.49	3.49
−3.00	−1.27	8.0	−0.63	2.90	1.69	1.36	2.32	3.19	4.37
		10.0	−0.39	2.85	1.67	1.36	2.31	3.19	4.36
		12.5	−0.21	2.77	1.64	1.34	2.28	3.15	4.30
		15.0	−0.08	2.67	1.60	1.32	2.24	3.10	4.24
		18.0	0.06	2.55	1.55	1.30	2.23	3.09	4.24
−2.00	−0.25	4.0	0.23	3.22	2.04	1.90	3.27	4.44	5.92
		5.0	0.35	3.23	2.02	1.88	3.24	4.40	5.87
		6.0	0.50	3.18	2.00	1.87	3.22	4.37	5.84
		8.0	0.70	3.10	1.95	1.85	3.19	4.34	5.80
		10.0	0.89	2.97	1.90	1.83	3.17	4.32	5.78
		12.5	1.05	2.83	1.84	1.80	3.14	4.29	5.76
		15.0	1.22	2.54	1.72	1.77	3.11	4.27	5.76
−1.77	−0.02	4.0	0.57	3.16	2.08	2.05	3.52	4.76	6.31
		5.0	0.75	3.12	2.05	2.04	3.50	4.74	6.30
		6.0	0.89	3.08	2.02	2.03	3.49	4.73	6.29
		8.0	1.10	2.98	1.96	2.00	3.46	4.69	6.25
		10.0	1.25	2.88	1.91	1.97	3.43	4.67	6.23
		12.5	1.44	2.68	1.81	1.94	3.39	4.64	6.21
		15.0	1.56	2.41	1.69	1.89	3.35	4.60	6.18
−1.54	0.22	4.0	0.99	2.97	2.04	2.19	3.77	5.10	6.76
		5.0	1.14	2.94	2.01	2.17	3.75	5.08	6.74
		6.0	1.28	2.90	1.98	2.16	3.74	5.07	6.74
		8.0	1.52	2.77	1.90	2.13	3.72	5.06	6.74
		10.0	1.65	2.66	1.83	2.09	3.67	5.01	6.69
		12.5	1.80	2.50	1.73	2.04	3.61	4.96	6.65
		15.0	1.94	2.18	1.57	1.96	3.54	4.89	6.61

Hence effective colors are much more sensitive than integrated colors to a change in the color–magnitude (c–m) diagram of a stellar population.

It is also relevant to note, from the figure, that effective colors do not necessarily relate monotonically to integrated colors. This is evident for example when looking at the trend of $\bar{B}-\bar{V}$ vs. $B-V$. While integrated colors become systematically redder with increasing metallicity, effective colors always reach a maximum and then reverse their trend becoming "bluer" beyond a critical value of [Fe/H]. The exact limit depends on the bandpasses, yet it tends to be higher as we move to infrared wavelengths (we verified for example that $\bar{V}-\bar{K}$ reverses beyond [Fe/H] ~ 0.5 while $\bar{B}-\bar{V}$ turns back for [Fe/H] ≥ -0.10).

This effect can be easily explained comparing qualitatively the B and V effective magnitudes of SSPs in Tables 1–3 with a typical c–m diagram. Increasing metallicity and/or age the "barycentre" of the population moves down to fainter magnitudes descending the red giant branch (RGB). At first, both $\bar{B}$ and $\bar{V}$ start fading, but $\bar{B}$ is fainter and reaches the knee at the onset of the subgiant branch (SGB) earlier respect to V. When this occurs $\bar{B}-\bar{V}$ turns back to the blue as $\bar{B}$ becomes nearly constant moving horizontally along the SGB while $\bar{V}$ continues to fade.

Comparing with the models of Buzzoni et al. (1992), a similar reasoning explains also the apparent bimodal trend of the Mg_2 index vs. $\bar{V}-\bar{I}$ found by Tonry et al. (1990; see their Fig. 9) without requiring an addition of a peculiar ongoing star formation.

The same arguments explain an opposite trend at extremely low metallicity, and now it is the infrared effective

Table 2a. SSP models for $s=2.35$ ($\eta=0.3$)

Log Z	[Fe/H]	Age (Gyr)	$\overline{V}$	$\overline{U}-\overline{V}$	$\overline{B}-\overline{V}$	$\overline{V}-\overline{R}$	$\overline{V}-\overline{I}$	$\overline{V}-\overline{J}$	$\overline{V}-\overline{K}$
−4.00	−2.27	8.0	−2.58	0.08	0.59	0.60	1.00	1.31	3.32
		10.0	−1.68	1.56	1.11	0.94	1.58	2.18	3.27
		12.5	−1.09	2.12	1.34	1.10	1.86	2.59	3.66
		15.0	−0.85	2.18	1.36	1.11	1.87	2.62	3.68
		18.0	−0.65	2.17	1.35	1.10	1.86	2.60	3.66
−3.00	−1.27	8.0	−0.76	3.07	1.77	1.42	2.41	3.33	4.55
		10.0	−0.55	3.05	1.76	1.43	2.43	3.35	4.59
		12.5	−0.36	2.95	1.72	1.40	2.39	3.29	4.51
		15.0	−0.26	2.88	1.69	1.38	2.34	3.24	4.43
		18.0	−0.14	2.79	1.65	1.36	2.31	3.19	4.37
−2.00	−0.25	4.0	0.18	3.35	2.12	2.00	3.44	4.67	6.22
		5.0	0.31	3.35	2.10	1.97	3.40	4.62	6.16
		6.0	0.44	3.31	2.08	1.96	3.39	4.61	6.15
		8.0	0.64	3.23	2.04	1.94	3.35	4.57	6.11
		10.0	0.82	3.11	1.99	1.93	3.34	4.55	6.09
		12.5	0.98	2.96	1.92	1.89	3.29	4.49	6.01
		15.0	1.14	2.71	1.83	1.87	3.26	4.46	5.99
−1.77	−0.02	4.0	0.52	3.29	2.17	2.16	3.69	4.99	6.61
		5.0	0.68	3.26	2.15	2.15	3.70	5.00	6.64
		6.0	0.83	3.21	2.11	2.14	3.68	4.98	6.62
		8.0	1.04	3.11	2.05	2.11	3.64	4.94	6.58
		10.0	1.19	3.02	2.00	2.08	3.61	4.91	6.54
		12.5	1.38	2.82	1.91	2.05	3.58	4.87	6.52
		15.0	1.51	2.55	1.79	2.01	3.53	4.82	6.47
−1.54	0.22	4.0	0.98	3.06	2.12	2.30	3.96	5.35	7.08
		5.0	1.12	3.04	2.10	2.29	3.96	5.36	7.11
		6.0	1.27	2.99	2.06	2.27	3.94	5.34	7.09
		8.0	1.50	2.86	1.97	2.24	3.91	5.32	7.09
		10.0	1.64	2.75	1.90	2.21	3.87	5.28	7.05
		12.5	1.79	2.58	1.80	2.15	3.80	5.20	6.97
		15.0	1.94	2.28	1.65	2.09	3.74	5.15	6.93

color $\bar{V}-\bar{K}$ that first turns to the red with decreasing [Fe/H] (see Fig. 2).

The overall dependence of the effective luminosity at the different bands on the distinctive integrated colors for SSPs is displayed in Figs. 3 and 4 respectively vs. $B-V$ and $V-K$. Some remarks can be drawn comparing the two figures. As a general trend, effective magnitudes tend to become fainter with increasing metallicity and/or age of the stellar population.

The dependence on metallicity arises from the fact that increasing [Fe/H] it increases both fuel consumption on the stellar main sequence (MS) via the CNO cycle, and opacity in the outer envelope of the stars in the RGB and asymptotic giant branch (AGB). For a given age this results in stars of slightly lower mass, fainter luminosity, and redder giant branches. Similarly, with increasing age the mass of the luminous stars decreases hence reducing the contribution of the MS.

To some extent, both effects are of comparable importance in modulating $l_{\rm eff}$, yet on the one hand changing age we act mainly on stellar MS introducing minor changes on colors, on the other, changes in metallicity affect more extensively the stellar temperature throughout the c–m diagram inducing a larger color variation. This being the case for red and infrared colors.

As shown in Fig. 4, thanks to its different dependence on age and metallicity $V-K$ better discriminates between the two effects while $B-V$ would not be so effective since $\bar{R}$ and $\bar{V}$ change very similarly both with age and [Fe/H].

Table 2b. SSP models for $s=2.35$ ($\eta=0.5$)

Log Z	[Fe/H]	Age (Gyr)	$\overline{V}$	$\overline{U}-\overline{V}$	$\overline{B}-\overline{V}$	$\overline{V}-\overline{R}$	$\overline{V}-\overline{I}$	$\overline{V}-\overline{J}$	$\overline{V}-\overline{K}$
-4.00	-2.27	8.0	-2.19	0.26	0.62	0.62	1.02	1.36	3.17
		10.0	-1.39	1.36	1.01	0.87	1.46	2.00	3.10
		12.5	-0.79	1.90	1.24	1.02	1.73	2.40	3.42
		15.0	-0.58	1.99	1.26	1.04	1.76	2.45	3.45
		18.0	-0.35	1.96	1.25	1.04	1.75	2.44	3.43
-3.00	-1.27	8.0	-0.54	2.89	1.68	1.36	2.30	3.17	4.34
		10.0	-0.31	2.84	1.67	1.35	2.30	3.17	4.33
		12.5	-0.13	2.76	1.63	1.33	2.26	3.12	4.26
		15.0	0.00	2.66	1.59	1.30	2.22	3.06	4.19
		18.0	0.15	2.54	1.55	1.29	2.20	3.04	4.18
-2.00	-0.25	4.0	0.33	3.20	2.04	1.91	3.29	4.46	5.95
		5.0	0.46	3.21	2.02	1.89	3.25	4.41	5.89
		6.0	0.60	3.17	2.00	1.87	3.22	4.38	5.85
		8.0	0.79	3.09	1.95	1.85	3.19	4.33	5.80
		10.0	0.99	2.95	1.89	1.82	3.16	4.30	5.76
		12.5	1.14	2.81	1.83	1.80	3.13	4.27	5.73
		15.0	1.31	2.52	1.71	1.76	3.09	4.24	5.72
-1.77	-0.02	4.0	0.68	3.13	2.07	2.06	3.53	4.78	6.34
		5.0	0.86	3.09	2.04	2.04	3.51	4.75	6.31
		6.0	0.99	3.05	2.01	2.03	3.49	4.73	6.30
		8.0	1.20	2.96	1.96	2.00	3.45	4.69	6.25
		10.0	1.35	2.86	1.90	1.97	3.42	4.65	6.22
		12.5	1.54	2.66	1.80	1.93	3.38	4.61	6.18
		15.0	1.66	2.39	1.68	1.88	3.32	4.56	6.14
-1.54	0.22	4.0	1.10	2.93	2.03	2.20	3.79	5.12	6.79
		5.0	1.26	2.90	2.00	2.18	3.76	5.10	6.77
		6.0	1.40	2.86	1.97	2.16	3.75	5.08	6.76
		8.0	1.62	2.74	1.89	2.13	3.72	5.05	6.74
		10.0	1.76	2.63	1.82	2.08	3.66	4.99	6.68
		12.5	1.91	2.47	1.72	2.03	3.60	4.93	6.62
		15.0	2.05	2.16	1.56	1.95	3.51	4.86	6.57

3.2. *Composite stellar populations*

The stronger dependence of effective colors on the morphological features of a c–m diagram enables us in principle to explore in finer detail the characteristics of a stellar aggregate. In particular, effective colors might evidence any presence of contamination in a SSP.

In view of a possible application of our results to the study of elliptical galaxies through the Tonry–Schneider method, the case of composite stellar populations must be accounted for. Although in consequence of a fast chemical evolution ellipticals contain a mainly coeval old SSP, at metallicity about or slightly larger than solar (Frogel et al. 1980; Burstein et al. 1984; Buzzoni et al. 1992), nevertheless, it is quite reasonable to expect also a minor contribution from metal-poor stars of Population II of nearly the same age (cf. for example the models of Arimoto & Yoshii 1987). While these stars are expected to have a negligible effect on visual and infrared integrated colors, it is likely that effective colors would better trace them.

A proper modelling of composite stellar populations is a difficult task, due to the increasing number of free parameters. We therefore preferred to consider only the possible relevant cases of mixes of two 15 Gyr SSPs with different metallicity spanning the whole range for [Fe/H] between -2.27 and $+0.22$.

Resulting $\bar{V}$, $\bar{R}$, and $\bar{I}$ vs. $V-K$ are displayed in Fig. 5. It is evident that the net effect of adding a blue metal-poor SSP to a bulk of red metal-rich stars is a brightening of the B, V effective magnitudes. Thus, at short wavelengths we should expect the larger deviation as compared with the case of a pure SSP.

Quite comfortingly, $\bar{I}$ is negligibly affected by the mix in the sense that its change vs. $V-K$ is nearly the same like changing [Fe/H] in a SSP. This is a great advantage as the relationship $\bar{I}$ vs. $(V-K)$ does not depend on the particu-

Table 3a. SSP models for $s=3.35$ ($\eta=0.3$)

Log Z	[Fe/H]	Age (Gyr)	$\bar{V}$	$\bar{U}-\bar{V}$	$\bar{B}-\bar{V}$	$\bar{V}-\bar{R}$	$\bar{V}-\bar{I}$	$\bar{V}-\bar{J}$	$\bar{V}-\bar{K}$
−4.00	−2.27	8.0	−2.43	0.03	0.55	0.55	0.88	1.13	3.16
		10.0	−1.50	1.50	1.07	0.89	1.47	2.02	3.07
		12.5	−0.90	2.07	1.31	1.05	1.76	2.46	3.49
		15.0	−0.67	2.12	1.32	1.06	1.78	2.49	3.52
		18.0	−0.46	2.11	1.31	1:06	1.77	2.47	3.49
−3.00	−1.27	8.0	−0.60	3.03	1.74	1.39	2.33	3.21	4.39
		10.0	−0.40	3.00	1.74	1.40	2.36	3.25	4.45
		12.5	−0.22	2.91	1.70	1.37	2.31	3.18	4.36
		15.0	−0.12	2.83	1.66	1.34	2.26	3.11	4.27
		18.0	0.01	2.73	1.62	1.31	2.22	3.06	4.19
−2.00	−0.25	4.0	0.34	3.29	2.11	1.99	3.41	4.62	6.16
		5.0	0.47	3.30	2.08	1.96	3.36	4.56	6.09
		6.0	0.60	3.26	2.06	1.94	3.34	4.54	6.07
		8.0	0.79	3.18	2.02	1.91	3.30	4.48	5.99
		10.0	0.97	3.05	1.96	1.89	3.27	4.45	5.96
		12.5	1.14	2.90	1.89	1.85	3.20	4.36	5.85
		15.0	1.29	2.65	1.80	1.82	3.17	4.33	5.82
−1.77	−0.02	4.0	0.69	3.21	2.14	2.13	3.65	4.92	6.53
		5.0	0.85	3.19	2.12	2.13	3.64	4.92	6.54
		6.0	0.99	3.15	2.09	2.11	3.63	4.90	6.53
		8.0	1.20	3.04	2.02	2.07	3.57	4.84	6.45
		10.0	1.35	2.95	1.97	2.04	3.53	4.79	6.40
		12.5	1.55	2.74	1.87	2.00	3.48	4.74	6.35
		15.0	1.68	2.48	1.75	1.95	3.42	4.66	6.27
−1.54	0.22	4.0	1.15	2.99	2.09	2.28	3.93	5.30	7.03
		5.0	1.29	2.96	2.07	2.27	3.92	5.30	7.04
		6.0	1.44	2.92	2.03	2.24	3.88	5.26	7.00
		8.0	1.67	2.79	1.94	2.21	3.85	5.23	6.98
		10.0	1.81	2.69	1.87	2.16	3.79	5.16	6.92
		12.5	1.97	2.50	1.76	2.10	3.70	5.06	6.79
		15.0	2.11	2.20	1.61	2.03	3.63	4.99	6.74

lar details of the composite stellar population providing a univocal comparison with observations. Moreover, $\bar{I}$ is the most favourable magnitude for determining the fluctuation distance with the Tonry–Schneider method as it gets the brightest absolute luminosity inducing therefore the largest and more easily detectable fluctuation on galactic surface brightness.

Due to their behavior, $\bar{V}$ and $\bar{R}$ would be effective in detecting the presence of a metal-poor stellar component in elliptical galaxies.

4. Surface-brightness fluctuations as distance estimator

4.1. Linking models and observations

The study of surface-brightness fluctuations in external galaxies and its possible application for measuring extragalactic distances has been successfully carried on in the last years by Tonry and colleagues (Tonry et al. 1990; Tonry & Schechter 1990; Tonry 1991). They have collected a number of observations of elliptical galaxies in the Virgo cluster, and in the Leo, Fornax and Eridanus groups. Supplementary observations include also Centaurus A and M 81, as well as galaxies in the M 31 system (M 32, NGC 205). Ellipticals were preferred to spirals because of a less complex stellar population that would ease the comparison with models allowing in principle a more accurate distance estimate.

At the light of current results, their inferred distance scale for galaxies stem from imperfect theoretical models for stellar populations derived from the revised Yale isochrones (Green et al. 1987) in Tonry et al. (1990). In particular, a leading point in their discussion is that I effective magnitudes are to be preferred in deriving distance

Table 3b. SSP models for $s=3.35$ ($\eta=0.5$)

Log Z	[Fe/H]	Age (Gyr)	$\overline{V}$	$\overline{U}-\overline{V}$	$\overline{B}-\overline{V}$	$\overline{V}-\overline{R}$	$\overline{V}-\overline{I}$	$\overline{V}-\overline{J}$	$\overline{V}-\overline{K}$
−4.00	−2.27	8.0	−2.03	0.20	0.58	0.56	0.90	1.17	2.97
		10.0	−1.21	1.30	0.97	0.81	1.34	1.83	2.88
		12.5	−0.60	1.84	1.20	0.97	1.62	2.25	3.23
		15.0	−0.39	1.93	1.23	0.99	1.66	2.31	3.27
		18.0	−0.17	1.90	1.21	0.99	1.65	2.30	3.25
−3.00	−1.27	8.0	−0.38	2.84	1.66	1.32	2.22	3.04	4.16
		10.0	−0.16	2.80	1.64	1.32	2.22	3.05	4.17
		12.5	0.03	2.71	1.61	1.29	2.18	2.99	4.10
		15.0	0.15	2.60	1.56	1.26	2.13	2.92	4.00
		18.0	0.30	2.48	1.52	1.24	2.11	2.90	3.98
−2.00	−0.25	4.0	0.50	3.14	2.02	1.90	3.25	4.40	5.87
		5.0	0.61	3.16	2.01	1.87	3.21	4.35	5.80
		6.0	0.75	3.11	1.98	1.85	3.17	4.30	5.74
		8.0	0.94	3.03	1.93	1.81	3.12	4.23	5.66
		10.0	1.14	2.89	1.87	1.78	3.08	4.18	5.60
		12.5	1.29	2.75	1.80	1.75	3.03	4.13	5.54
		15.0	1.47	2.46	1.68	1.71	2.99	4.09	5.52
−1.77	−0.02	4.0	0.86	3.05	2.05	2.04	3.48	4.70	6.24
		5.0	1.03	3.01	2.01	2.01	3.45	4.66	6.19
		6.0	1.16	2.98	1.99	2.00	3.43	4.64	6.18
		8.0	1.37	2.89	1.92	1.96	3.38	4.57	6.10
		10.0	1.51	2.79	1.87	1.92	3.33	4.52	6.05
		12.5	1.72	2.58	1.76	1.88	3.27	4.46	5.99
		15.0	1.84	2.31	1.63	1.82	3.20	4.38	5.91
−1.54	0.22	4.0	1.28	2.86	2.00	2.18	3.75	5.07	6.72
		5.0	1.43	2.83	1.97	2.15	3.71	5.02	6.67
		6.0	1.57	2.79	1.94	2.13	3.69	4.99	6.64
		8.0	1.79	2.67	1.85	2.09	3.64	4.94	6.60
		10.0	1.92	2.57	1.78	2.04	3.57	4.87	6.52
		12.5	2.08	2.39	1.68	1.97	3.48	4.76	6.41
		15.0	2.22	2.08	1.51	1.88	3.39	4.68	6.35

moduli because of their constancy versus both age and [Fe/H], contrary to $\bar{V}$ and $\bar{R}$. Now, just a glance to Fig. 4 makes clear that this assumption cannot be longer supported by the present analysis.

Indeed, there cannot be any realistic physical reason to induce such a striking difference in the trend of $\bar{I}$ and, for example, that of the side band $\bar{R}$. Quite peculiarly in fact, this would require that the effective stellar contributors emitting at 8000 Å in a SSP should be almost decoupled from those contributing at 6500 Å in clear disagreement for instance with the trend for $N_{\rm eff}$ envisaged in Fig. 1.

It is fair to note that our conclusions are supported by the supplementary observations of $\bar{I}$ vs. $V-I$ made by Tonry (1991). In that work he correctly pointed out the apparent discrepancy, with his adopted models displaying an opposite trend respect to observations. We are inclined to believe that the rough constancy of $\bar{I}$ in the models of Tonry et al. (1990) artificially stems from a too scanty treatment of the late stellar evolutionary stages in their theoretical populations contributing to the infrared light.

On the basis of the new set of models available, we attempted to refine distance estimates previously inferred for galaxies in the Tonry et al. sample. As observations were all taken in the Cousins system, while Buzzoni's (1989) models adopted Johnson's bandpasses, a transformation was performed by adopting Bessell's (1979) equations. Although these transformation equations are derived from stellar observations we have verified that they can be suitable for galaxies too as galaxies closely match the stellar locus in the $(\bar{V}-\bar{R})$ vs. $(\bar{V}-\bar{I})$ diagram. Thus we have

$$R_{\rm J}=R_{\rm C}-0.61(V-R_{\rm C})-0.13,$$

$$I_{\rm J}=I_{\rm C}-0.20(V-I_{\rm C})-0.16, \qquad (7a, b)$$

Table 4. Effective contributors for SSP models with R-HB ($s=2.35$, $\eta=0.3$)

Log Z	[Fe/H]	Age	N_{TOT}	N^U_{eff}	N^B_{eff}	N^V_{eff}	N^R_{eff}	N^I_{eff}	N^J_{eff}	N^K_{eff}
−4.00	−2.27	8.0	6.36+0	7.78−4	1.13−3	1.02−3	9.23−4	8.96−4	9.28−4	2.61−4
		10.0	8.30+0	5.26−3	3.37−3	2.10−3	1.53−3	1.27−3	1.07−3	7.02−4
		12.5	9.40+0	1.31−2	6.34−3	3.38−3	2.22−3	1.73−3	1.35−3	9.19−4
		15.0	1.01+1	1.65−2	7.75−3	4.15−3	2.75−3	2.15−3	1.68−3	1.15−3
		18.0	1.11+1	1.88−2	8.95−3	4.93−3	3.34−3	2.64−3	2.08−3	1.45−3
−3.00	−1.27	8.0	7.82+0	3.42−2	1.09−2	4.15−3	2.13−3	1.40−3	9.76−4	6.15−4
		10.0	8.55+0	3.90−2	1.28−2	4.97−3	2.57−3	1.69−3	1.18−3	7.38−4
		12.5	9.76+0	4.11−2	1.43−2	5.85−3	3.13−3	2.11−3	1.49−3	9.52−4
		15.0	1.22+1	4.04−2	1.48−2	6.35−3	3.52−3	2.41−3	1.74−3	1.13−3
		18.0	1.36+1	4.02−2	1.57−2	7.07−3	4.04−3	2.83−3	2.07−3	1.37−3
−2.00	−0.25	4.0	5.43+0	7.53−2	2.84−2	8.14−3	2.61−3	1.23−3	6.99−4	3.74−4
		5.0	6.48+0	8.05−2	3.02−2	9.08−3	3.04−3	1.46−3	8.39−4	4.52−4
		6.0	7.46+0	8.45−2	3.26−2	1.01−2	3.45−3	1.67−3	9.62−4	5.18−4
		8.0	9.18+0	8.75−2	3.59−2	1.19−2	4.20−3	2.06−3	1.21−3	6.55−4
		10.0	1.08+1	8.66−2	3.89−2	1.38−2	5.00−3	2.49−3	1.47−3	8.00−4
		12.5	1.40+1	8.17−2	4.08−2	1.57−2	5.97−3	3.04−3	1.82−3	1.01−3
		15.0	1.52+1	7.12−2	4.19−2	1.78−2	6.99−3	3.59−3	2.16−3	1.21−3
−1.77	−0.02	4.0	6.07+0	8.34−2	3.62−2	1.03−2	2.95−3	1.30−3	7.16−4	3.75−4
		5.0	7.16+0	8.93−2	3.97−2	1.17−2	3.40−3	1.50−3	8.24−4	4.29−4
		6.0	8.23+0	9.44−2	4.33−2	1.34−2	3.96−3	1.76−3	9.69−4	5.02−4
		8.0	1.03+1	9.64−2	4.75−2	1.59−2	4.93−3	2.23−3	1.24−3	6.44−4
		10.0	1.20+1	9.33−2	4.95−2	1.78−2	5.75−3	2.64−3	1.48−3	7.72−4
		12.5	1.42+1	8.59−2	5.17−2	2.07−2	6.99−3	3.25−3	1.83−3	9.59−4
		15.0	1.69+1	7.07−2	5.00−2	2.26−2	8.05−3	3.80−3	2.17−3	1.14−3
−1.54	0.22	4.0	6.99+0	8.87−2	4.80−2	1.47−2	3.75−3	1.51−3	7.80−4	3.85−4
		5.0	8.54+0	9.41−2	5.19−2	1.64−2	4.26−3	1.71−3	8.80−4	4.30−4
		6.0	9.78+0	9.84−2	5.59−2	1.86−2	4.98−3	2.02−3	1.04−3	5.11−4
		8.0	1.12+1	9.80−2	6.07−2	2.25−2	6.28−3	2.56−3	1.32−3	6.40−4
		10.0	1.35+1	9.22−2	6.13−2	2.48−2	7.31−3	3.03−3	1.58−3	7.61−4
		12.5	1.73+1	8.38−2	6.17−2	2.79−2	8.79−3	3.72−3	1.96−3	9.53−4
		15.0	1.85+1	6.74−2	5.82−2	3.09−2	1.05−2	4.49−3	2.36−3	1.14−3

and

$$(V-R_J)=1.61(V-R_C)+0.13,$$

$$(V-I_J)=1.20(V-I_C)+0.16. \quad \text{(8a, b)}$$

Note that since transformations are applied to *effective magnitudes*, they must use *effective colors*, that are much redder than the integrated ones. Therefore, larger corrections to Cousins magnitudes would be introduced by using integrated colors, with Johnson magnitudes about 0.5–0.7 mag brighter. A direct comparison of our models for 15 Gyr SSPs with the composite locus of Tonry et al. (1990, see their Fig. 4) transformed in the Johnson $R-I$ plane is made in Fig. 6.

According to the discussion in Sect. 3, fluctuation distances were derived for galaxies considering $\bar{V}$, $\bar{R}$, and $\bar{I}$ magnitudes coupled with $V-K$ colors. Infrared photometry for most of the galaxies was taken from Frogel et al. (1978), and Persson et al. (1979). Where only $\bar{I}_C$ magnitude was available for a galaxy, the magnitude transformation was derived through Eq. (7) adopting the mean effective colors derived from Tonry et al. (1990), i.e. $\bar{V}-\bar{R}_C=0.92\pm0.14$, and $\bar{V}-\bar{I}_C=2.36\pm0.23$.

In agreement with Tonry et al. (1990), we can confirm that a detectable presence of metal-poor stars appears in the elliptical galaxies. Plotting the data for galaxies in the Virgo cluster in the $(\bar{V}-\bar{I})$ vs. $(\bar{V}-\bar{R})$ plane (see Fig. 7) we clearly see that points clump at exceedingly low metallicities (discrepant respect to what expected from integrated $V-K$), and slightly off the strip expected for SSPs. Most of this displacement is induced by an excess $\bar{V}$ luminosity. Like in Fig. 6 of Tonry et al. (1990) we can fully match data by adding to metal-rich SSPs a fraction of 5–15% of the total V light provided by a [Fe/H] = −2.27 population 15 Gyr old. Indeed, we could conclude that effective colors give so far the more direct and confident evidence of a metal-poor stellar component in elliptical galaxies.

4.2. *Inferring extragalactic distances*

New distance moduli at I derived for galaxies in the Tonry et al. sample are listed in Table 6. There, elliptical galaxies are assumed to be properly described by 15 Gyr Salpeter SSP models. As previously discussed, such a simplification holds as far as red or infrared magnitudes and colors are concerned. In this table all magnitudes have been corrected for reddening according to the original sources of photometry and given in the Johnson system.

Resting on the models of Fig. 4, we should note that a feedback links the assumption about galactic age and the

Table 5. SSP models for globular clusters ($s=2.35$, $\eta=0.3$)

Log Z	[Fe/H]	Age (Gyr)	$\bar{V}$	$\bar{U}-\bar{V}$	$\bar{B}-\bar{V}$	$\bar{V}-\bar{R}$	$\bar{V}-\bar{I}$	$\bar{V}-\bar{J}$	$\bar{V}-\bar{K}$
			I-HB morphology						
−4.00	−2.27	8.0	−2.58	0.09	0.60	0.61	1.01	1.32	3.34
		10.0	−1.68	1.57	1.11	0.95	1.59	2.21	3.30
		12.5	−1.09	2.09	1.34	1.12	1.88	2.63	3.71
		15.0	−0.85	2.12	1.34	1.13	1.90	2.66	3.73
		18.0	−0.65	2.09	1.32	1.13	1.90	2.65	3.71
−3.00	−1.27	8.0	−0.76	3.06	1.76	1.43	2.42	3.33	4.56
		10.0	−0.55	3.01	1.75	1.43	2.43	3.36	4.60
		12.5	−0.36	2.79	1.69	1.41	2.40	3.31	4.53
		15.0	−0.27	2.52	1.58	1.40	2.38	3.28	4.48
		18.0	−0.16	2.56	1.61	1.39	2.35	3.23	4.41
			B-HB morphology						
−4.00	−2.27	8.0	−2.60	0.11	0.62	0.63	1.04	1.36	3.36
		10.0	−1.72	1.60	1.13	0.96	1.61	2.22	3.31
		12.5	−1.14	2.17	1.36	1.12	1.88	2.62	3.69
		15.0	−0.91	2.26	1.39	1.13	1.90	2.64	3.70
		18.0	−0.71	2.27	1.38	1.12	1.88	2.62	3.67
−3.00	−1.27	8.0	−0.76	2.99	1.75	1.43	2.42	3.34	4.57
		10.0	−0.55	2.77	1.70	1.45	2.46	3.39	4.63
		12.5	−0.39	2.77	1.69	1.43	2.43	3.34	4.55
		15.0	−0.31	2.95	1.73	1.40	2.38	3.27	4.46
		18.0	−0.20	3.04	1.72	1.38	2.33	3.21	4.38

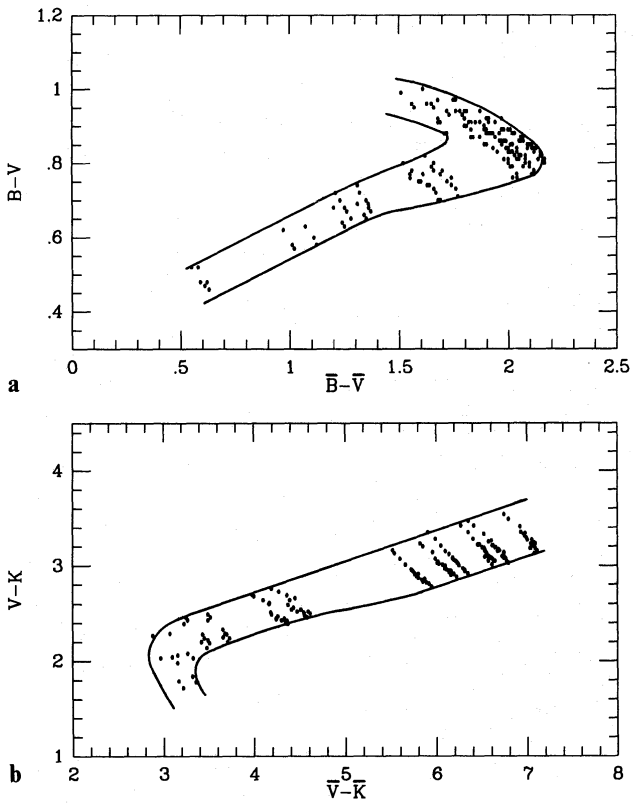

Fig. 2a and b. Effective and integrated colors for the SSPs of Tables 1–3. It is evident in **a** the hooked feature with $\bar{B}-\bar{V}$ turning back to the blue with increasing metallicity. The same happens to $\bar{V}-\bar{K}$ in **b**, but in the opposite sense and at low metallicity (see text for discussion). Both $B-V$ and $V-K$ are from Buzzoni (1989)

inferred distance scale; this is in the sense that assuming a younger age in the fitting models we predict larger distances, and therefore an older age for the Universe (i.e. a lower Hubble constant). A distance modulus excess of 0.4 mag (i.e. larger distances by 20%) would require the adoption of an age of 10 Gyr instead of 15 for the galaxies, while a change in the IMF respect to the Salpeter case would lead to increasing distances [$\Delta(m-M)_I=+0.12$] for giant-dominated SSPs ($s=1.35$) or conversely $\Delta(m-M)_I=-0.27$ for $s=3.35$.

Nine of the galaxies in Virgo measured in I by Tonry et al. (1990) have also reliable $V-K$ integrated colors. From this sample we derive the distance modulus of the Virgo cluster, i.e. $(m-M)_0=30.87\pm0.46$ or $D=15.3\pm3.5$ Mpc. The quoted uncertainty should be taken not as an error bar but rather as a measure of the finite dimensions of the cluster. Actually, we see from Table 6 that the distance of NGC 4365 at the more distant limit of the cluster is nearly twice the distance of NGC 4636.

Due to a number of error sources, we believe that a realistic $1-\sigma$ estimate of the internal consistency in our derived distance moduli could be ±0.2 mag; this includes a 0.15 mag uncertainty in the photometric system transformation, and a 0.10 mag observational error. This estimated error yields a 10% uncertainty on the inferred distances to the galaxies. It is worth stressing however that this value disregards any possible error in the models that could lead in principle to an even larger systematic shift of the distance scale.

Through a similar procedure, we estimated the distance moduli of the galaxies in the Leo, Fornax and Eridanus groups (always resting on $\bar{I}$ magnitudes and $V-K$). From two galaxies in Leo (NGC 3377 and NGC 3379) we obtain $(m-M)_0=29.93$, while for six galaxies in Fornax and three galaxies in Eridanus a similar distance is derived i.e. $(m-M)_0=30.72$ and 30.73, respectively. This places Leo at 9.7 Mpc, the Fornax group at 14.1 Mpc, and Eridanus at 14.2 Mpc. For both Fornax and Eridanus we derive an extension of ±2.5 Mpc (1-σ dispersion in the distances) so that the two subgroups might possibly be in contact.

These new results indicate distances in general agreement (within $\pm5\%$) with Tonry (1991), with the exception of Eridanus, for which we found a 15% closer distance, placing it nearly at the same distance of Fornax. This agrees with the fact that the two groups might be in close interaction (Willmer et al. 1989). The discrepancy with Tonry (1991) could arise because of the large $V-K$ of the three galaxies accounted that places them at the extreme edge of the $\bar{I}$ calibration, a region where our SSP models are quite different as compared to those of Tonry et al. (1990; cf. Fig. 6).

4.3. Local calibrators

One main difficulty pointed out in Tonry et al. (1990) is that on the basis of their models a fluctuation distance of 0.85 Mpc is derived for M 32. As this value seemed too discordant with other current estimates, that yield 0.7 Mpc, in their work they empirically corrected the effective magnitudes in order to match their extragalactic distance scale. It is fair to note that with the present models we obtain from the same data $(m-M)_I=24.35$, that would place M 32 at 0.74 ± 0.07 Mpc in perfect agreement with Van den Bergh's (1989) review indicating for the M 31 system a mean distance modulus of 24.3 ± 0.1. This result reinforces our confidence on previous conclusions about selfconsistency of our theoretical framework. It is clear that a successful calibration of the local stellar systems is an unavoidable step to confidently extend the method to cosmological distances.

An alternative test to effectively check performances of the Tonry–Schneider method concerns the Galactic globular clusters. Indeed, they might be an important milestone for a fine calibration of the method in the local framework. Globulars are close enough that c–m diagram of their stars can be directly obtained in their outermost regions, while

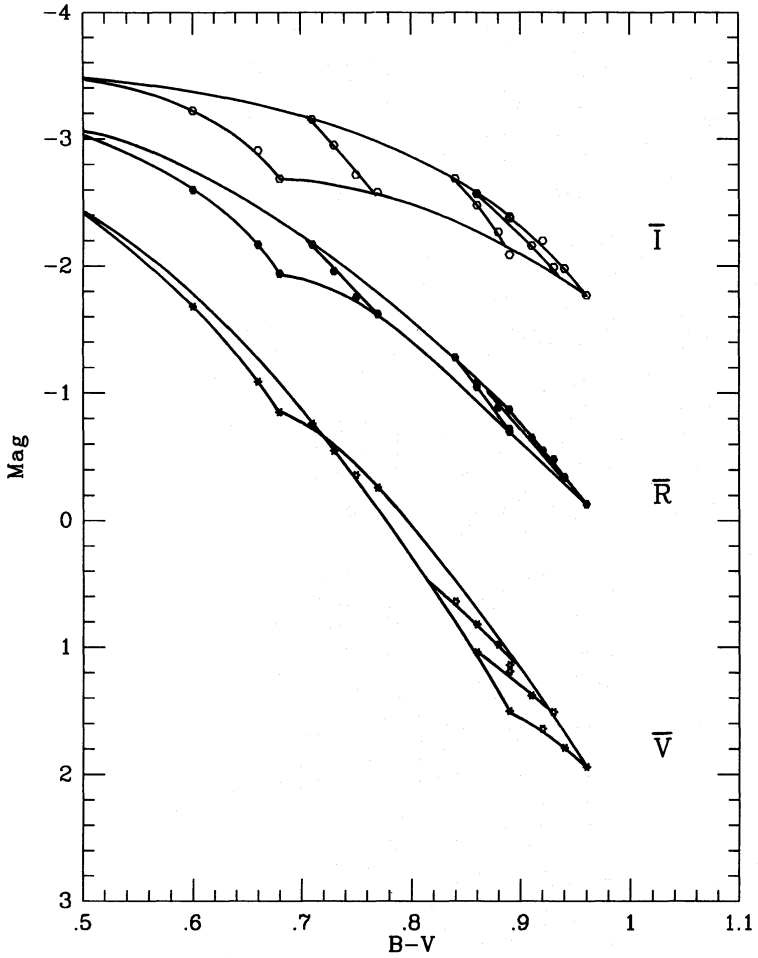

Fig. 3. Effective magnitudes in the Johnson V, R, and I bands of SSPs in Table 2a vs their integrated $B-V$. The upper envelope for the models in the different bands is for 8 Gyr populations, while lower envelope is for 15 Gyr. Lines within the envelopes trace time evolution of populations with fixed metallicity. Note the complex behaviour of $\bar{V}$ at low metallicity

to some extent observations of the core regions are of difficulty comparable to extragalactic surface photometry.

An excellent opportunity to verify the fluctuation distance of a globular cluster is provided by the complete B, V photometry of a sample of 10000 stars in M 3 (Buonanno et al. 1986, 1988). Authors performed deep photometry down to B 22nd mag in a ring of the cluster between 3.5′ and 6′ from the centre. Virtually all stars within the magnitude limit were detected and measured reaching about three magnitudes down the MS turn-off point so that we estimate that only a negligible fraction (i.e. less than 2%) of the total light of the cluster in the ring has been missed.

Using this sample we accomplished a simulation of what we could obtain observing the same zone of the cluster without resolving stars but only detecting the resulting surface mottling. Operationally, the ring was divided into ten sectors of equivalent area containing about 1000 stars each, and integrated flux was calculated for each of them. From the ten values we derived the mean and the relative variance according to the left hand term in Eq. (4). Different attempts had been performed for different choices of the sectors. This is equivalent to simulate repeated observations of statistically similar objects, all taken at the same distance, and allows therefore to estimate the internal error in the method deriving the true distance modulus.

The observed effective magnitudes of the M 3 stellar population resulted $\bar{m}_B = 16.15 \pm 0.34$, and $\bar{m}_V = 14.74 \pm 0.32$. The error bars reported are directly related to the total number of stars in our sample (i.e. 10000 stars) and their absolute size would therefore decrease with increasing the accounted fraction of the cluster. For comparison, and to check our procedure simulating observations, we calculated $\bar{m}_B$ and $\bar{m}_V$ more directly from the whole stellar sample by means of the ratio $\sum l^2 / \sum l$ as in the second term of Eq. (4). We obtained $\bar{m}_B = 16.13$ and $\bar{m}_V = 14.77$ in good agreement with previous estimates.

Assuming [Fe/H] $= -1.67$ and $E(B-V) = 0.01$ (Zinn 1980), and adopting an I-HB morphology from models in Table 5 we derive

$$(m-M)_B = 15.15 - 1.8 \log(t_9/15),$$
$$(m-M)_V = 15.21 - 1.8 \log(t_9/15), \qquad (9a, b)$$

where t_9 is the adopted age for the cluster, in Gyr. Buonanno et al. (1989) attribute to M 3 an age of 18.7 Gyr with a quoted uncertainty of ± 3 Gyr. Accounting for this, and combining the B and V relations we obtain

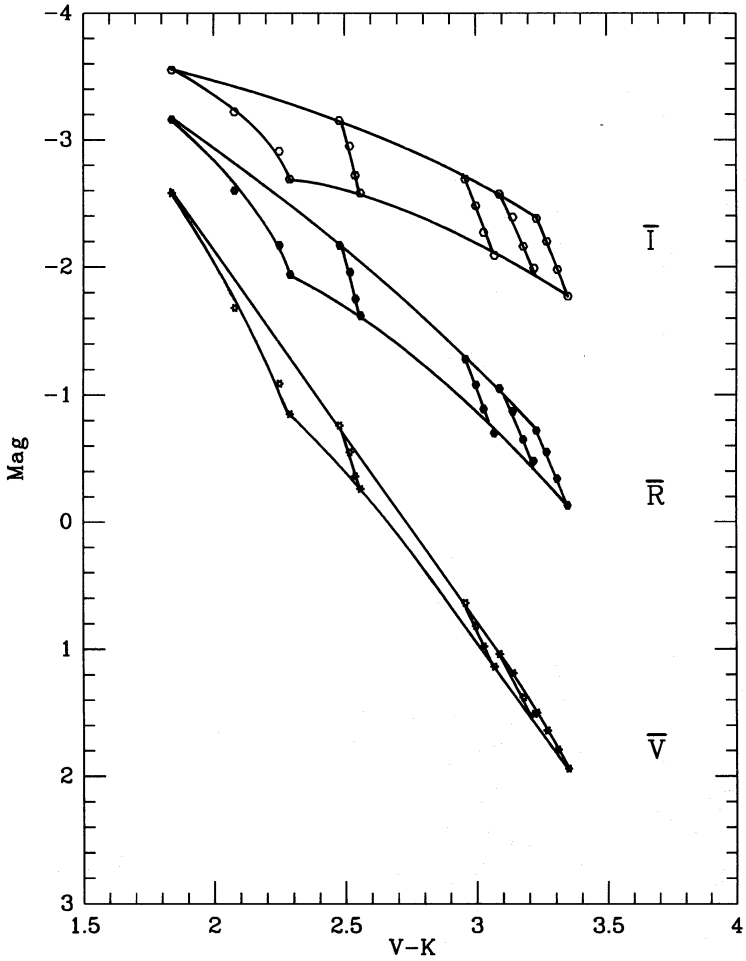

Fig. 4. Same as Fig. 3, but versus integrated $V-K$

$(m-M)_0 = 15.01 \pm 0.13$ (the formal error includes the B, V relations and the quoted age uncertainty) in excellent agreement with other current estimates that give $(m-M)_0 = 15.00$ (Harris & Racine 1979).

We conclude therefore that the method is totally successful in deriving an accurate estimate of the distance of M 3. Moreover, in its direct application to distant galaxies we would not expect a substantial loose of efficiency providing to collect signal enough to minimize the contribution to the scatter due to photon statistics, as discussed in Tonry & Schneider (1988). In addition, for galaxies we would take advantage of the larger statistics in stellar counts reducing therefore even more the observational uncertainty on $l_{\rm eff}$.

5. Conclusions

In this work we have focused our attention on some features related to the statistical properties of stellar populations. We introduced the concept of effective stellar contributors $N_{\rm eff}$, and effective luminosity $l_{\rm eff}$ of a stellar aggregate. These two quantities are tightly related, and are the primary parameters modulating the intrinsic statistical scatter of a pixel-to-pixel surface photometry of a galaxy (once other effects due to effective point spread functions are removed). The scatter increases with brightening the "barycentre" of the population in a c–m diagram adopting a luminosity-weighted average on stars.

We demonstrated that the number of effective contributors allows us to provide a measure of the crowding expected at a given wavelength when observing a stellar aggregate. The extreme ultraviolet (shortward of 2000 Å) is a preferred range where we might hope to resolve (blue) stars in a distant galaxy, and even see through its body.

The effective luminosity and number contributors in SSPs have been calculated from a wide set of models based on Buzzoni's (1989) code for population synthesis, and also the case of composite stellar populations has been accounted for. The results have been applied to the Tonry–Schneider (1988) method on the study of galaxy surface-brightness fluctuations deriving new distances for galaxies in the Virgo cluster, and in the Leo, Fornax, and Eridanus groups previously observed by Tonry and colleagues. New determinations are in general agreement within 5% with those of Tonry (1991) placing the Leo group at 9.7 Mpc, Fornax at 14.1 Mpc, Eridanus at 14.2 Mpc, and Virgo at 15.3 Mpc. Only the distance of the Eridanus group is sensibly decreased. This places it close

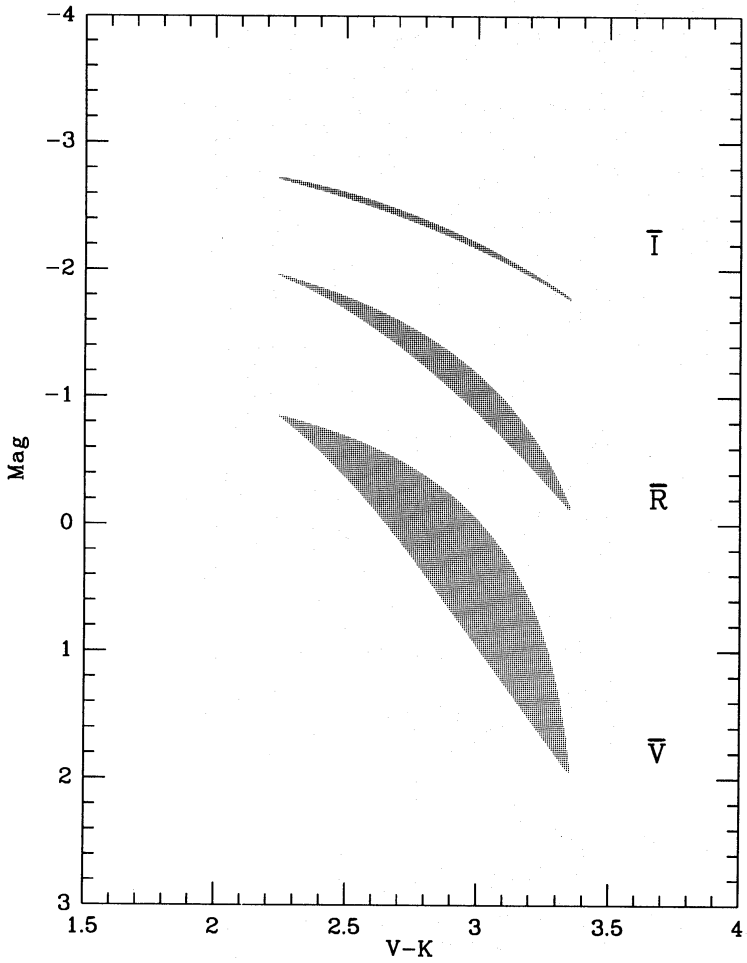

Fig. 5. Effective magnitudes for composite stellar populations. Each shaded area is defined by the envelopes at the different bands of any possible stellar combination from a mixture of 15 Gyr SSPs listed in Table 2a. For $\bar{V}$ and $\bar{R}$, the composite population always results in a brighter effective luminosity at a given $V-K$, with models lying in the figure above the loci expected for SSPs (i.e. the lower edge in each envelope, cf. also Fig. 4). The opposite trend is found for $\bar{I}$, but with negligible departure of composite models from the loci for SSPs

to Fornax, a system to which it might be gravitationally tied.

The reliability of the Tonry–Schneider method has been discussed in determining also the distance of local stellar systems. The case of M 32 has been discussed in detail deriving $D=0.74\pm0.07$ Mpc, in excellent agreement with the accepted distance of the M 31 system. This removes the apparent discrepancy pointed out by Tonry et al. (1990) when matching this primary distance calibrator.

The distance of the Galactic globular cluster M 3 has been derived by applying the method of surface-brightness fluctuations to the complete sample of 10000 stars observed by Buonanno et al. (1986, 1988). A distance modulus $(m-M)_0=15.01\pm0.13$ is found fully confirming the other current estimates based on the study of the stellar c–m diagram.

Although beyond the immediate scope of this work, it could be worth spending a word about the natural application of the Tonry–Schneider method for cosmological purposes in order to determine a consistent extragalactic distance scale. As we noted in the previous section, there is a direct link between the assumed age of the galaxies and their inferred fluctuation distance scale. The younger is the adopted age, the farther are placed galaxies. As this has a direct impact on the determination of the Hubble constant (and therefore on the age of the Universe), it is clear that we have to be self-consistent, and galaxies cannot be older than the Hubble time, H_0^{-1}, in a Friedmann cosmology.

Considering the Virgo cluster for instance, one might reasonably assume its true cosmological velocity of recession between 1144 ± 18 km s^{-1} (Sandage & Tammann 1990) and 1333 ± 75 km s^{-1} (Faber et al. 1989). At the distance of 15.3 ± 1.5 Mpc this leads respectively to $H_0=75\pm8$ or 87 ± 10 km s^{-1} Mpc^{-1}. Accordingly, the Universe could be older than $T_0=14.6$ or 12.7 Gyr at most. In both cases, our main hypothesis about a present age of galaxies of 15 Gyr is not in drastic conflict. Yet, by slightly decreasing the value and iterating we would increase distances (because of brighter reference effective magnitudes), then decreasing the inferred H_0. The Universe would thus become slightly older, and again we would eventually converge toward a fair estimate about 13–15 Gyr for its age.

Nevertheless, it remains to consider with attention the fact that the age which M 3 seems to firmly point to is clearly beyond the fiducial range (indeed a well established

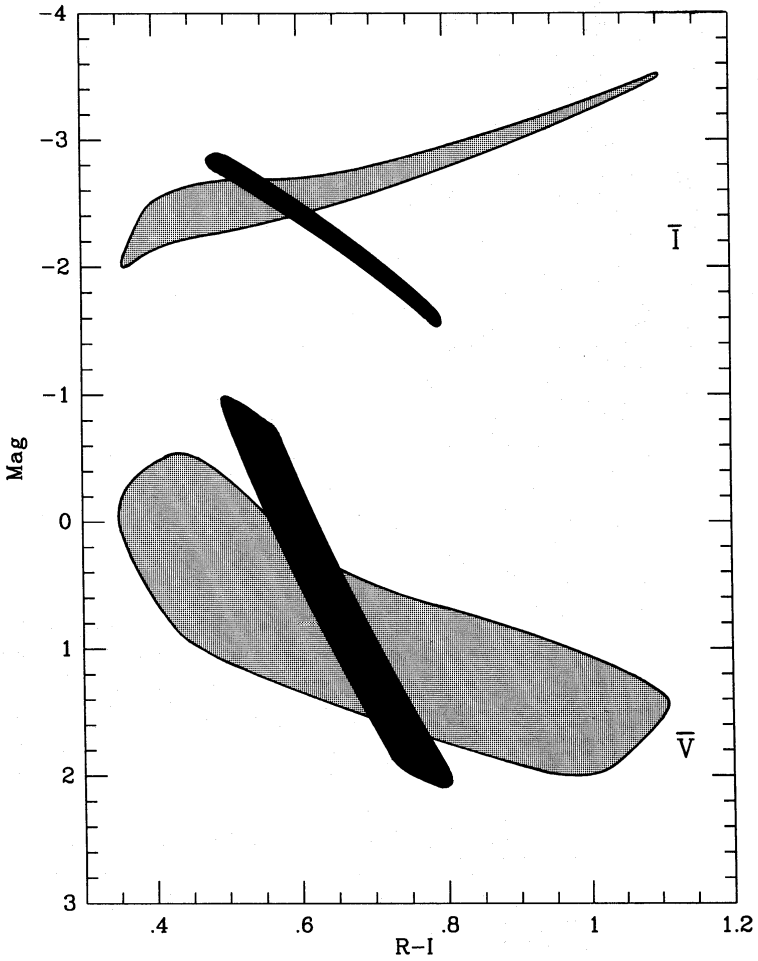

Fig. 6. Comparison between the whole set of 15 Gyr models in Tables 1–3 (black strips) and the composite locus for the models of Tonry et al. (1990) (green areas). Both colors and effective magnitudes are in the Johnson system

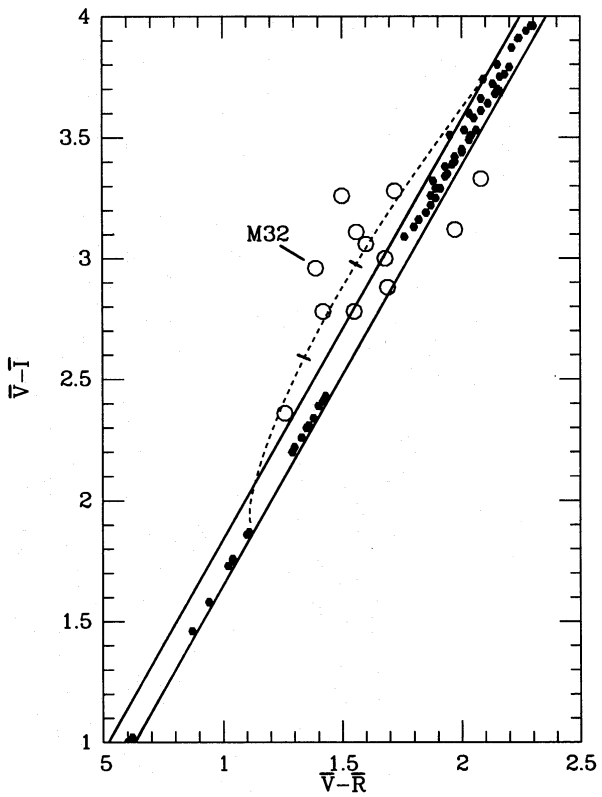

issue when dealing with globular clusters). It is hard to say, at the present status of the art, if this apparent discrepancy might be fully reconciled within the statistical uncertainties in the method [with $t_9 = 14$ in Eq. (9) we would lead to $(m-M)_0 = 15.23$] or it is rather opening to more exotic solutions for the cosmological scenario with T_0 possibly exceeding H_0^{-1} (Fukugita et al. 1990; Buzzoni et al. 1993).

Fig. 7. Comparison between effective colors expected for the SSP models in Tables 1–3 and observations by Tonry et al. (1990) of elliptical galaxies in the Virgo cluster (magnitudes are dereddened and transformed to the Johnson system). The supplementary point for M 32 is also marked. Galaxies seem to lie at exceedingly low metallicities with respect to SSP models with similar integrated colors. The reason is an excess $\bar{V}$ luminosity causing bluer effective colors. As discussed in the text, this might be induced by the contamination of metal-poor stellar component. The dashed line displays the change expected for a 15 Gyr Salpeter SSP with [Fe/H] = +0.22 by adding an increasing fraction of a similar metal-poor SSP with [Fe/H] = −2.27. Marked along the curve is a 10% and 20% total V contribution of the metal-poor population moving to bluer colors

Table 6. Data and derived distances of galaxies

NGC	$V-K$	$\overline{m}_V$	$\overline{m}_R$	$\overline{m}_I$	$\overline{V}-\overline{R}$	$\overline{V}-\overline{I}$	$(m-M)_o$	D(Mpc)	Ref.
221	3.00	25.14	23.75	22.18	1.39	2.96	24.35	0.74	(1)
				Fornax Group					
1344	3.16			28.76			30.80	14.5	(2)
1379	3.10			29.01			31.10	16.6	(2)
1380	3.29			28.78			30.65	13.5	(2)
1387	3.56			28.80			30.00	10.0	(2)
1399	3.41			29.06			30.70	13.8	(2)
1404	3.26			29.13			31.05	16.2	(2)
				Eridanus Group					
1395	3.34			29.39			31.20	17.4	(2)
1400	3.53			29.13			30.40	12.0	(2)
1407	3.52			29.29			30.60	13.2	(2)
				Leo Group					
3377	3.03			27.83			30.00	10.0	(2)
3379	3.30	31.21	29.71	27.95	1.50	3.26	29.85	9.3	(1)
				Virgo Cluster					
4365	3.35	32.36	31.10	30.00	1.26	2.36	31.80	22.9	(1)
4374	3.34	32.02	30.60	29.24	1.42	2.78	31.05	16.2	(1)
4406	3.29	32.11	30.56	29.33	1.55	2.78	31.20	17.4	(1)
4458	3.06	31.85	29.88	28.73	1.97	3.12	30.85	14.8	(1)
4468	3.01	31.21	29.53	28.21	1.68	3.00	30.40	12.0	(1)
4472	3.32	32.26	30.54	28.98	1.72	3.28	30.80	14.5	(1)
4552	3.37	31.69	30.00	28.81	1.69	2.88	30.50	12.6	(1)
4578	3.14	32.03	30.47	28.92	1.56	3.11	30.95	15.5	(1)
4636	3.49			28.84			30.30	11.5	(1)

(1): Tonry, Ajhar and Luppino (1990); (2): Tonry (1991)

Acknowledgements. It is a pleasure to thank Luis Carrasco for enjoyable discussions and a careful reading of the preliminary version of this paper. The anonymous referee is also acknowledged for his/her illuminating comments that helped refining the analysis of the present results. Mr. S. Cantù at OAB performed the excellent set up of the photographic material of the figures.

References

Arimoto N., Yoshii Y., 1987, A&A 173, 23
Bessell M.S., 1979, PASP 91, 589
Buonanno R., Corsi C.E., Fusi Pecci F., 1989, A&A 216, 80
Buonanno R., Buzzoni A., Corsi C.E., Fusi Pecci F., Sandage A.R., 1986, Mem. SAIt 57, 391
Buonanno R., Buzzoni A., Corsi C.E., Fusi Pecci F., Sandage A.R., 1988, in: Grindlay J.E., Philip A.G. (eds.) The Harlow-Shapley Symp. on Globular Clusters in Galaxies. Kluwer, Dordrecht, p. 621
Burstein D., Faber S.M., Gaskell C.M., Krumm N., 1984, ApJ 287, 586
Buzzoni A., 1988, in: Kron R.G., Renzini A. (eds.) Erice Workshop, Towards Understanding Galaxies at Large Redshift. Kluwer, Dordrecht, p. 61
Buzzoni A., 1989, ApJS 71, 817
Buzzoni A., Chincarini G., Molinari E., 1993, ApJ (in press)
Buzzoni A., Gariboldi G., Mantegazza L., 1992, AJ 103, 1814
Faber S.M., Wegner G., Burstein D., Davies R.L., Dressler A., Lynden-Bell D., Terlevich R.J., 1989, ApJS 69, 763
Freedman W., 1988, AJ 96, 1248
Freedman W., 1989, AJ 98, 1285
Frogel J.A., Persson S.E., Aaronson M., Matthews K., 1978, ApJ 220, 75
Frogel J.A., Persson S.E., Cohen J.G., 1980, ApJ 240, 785
Fukugita M., Takahara F., Yamashita K., Yoshii Y., 1990, ApJ 361, L4
Green E.M., Demarque P., King C.R., 1987, The Revised Yale Isochrones and Luminosity Functions. New Haven, Yale

Harrin W.E., Racine R., 1979, ARA&A 17, 241
Hill R.S., Hill J.K., Landsman W.B., Bohlin R.C., Cheng K.P., 1992, ApJ 395, L17
Laget M., Burgarella D., Milliard B., Donas J., 1992, A&A 259, 510
Mould J., Kristian J., da Costa G., 1983, ApJ 270, 471
Mould J., Kristian J., da Costa G., 1984, ApJ 278, 575
Persson S.E., Frogel J.A., Aaronson M., 1979, ApJS 39, 61
Reimers D., 1975, Mem. Soc. Roy. Sci. Liège, 6th Ser. 8, 369
Sandage A., Tammann G.A., 1990, ApJ 365, 1
Tonry J.L., 1991, ApJ 373, L1
Tonry J.L., Schneider D.P., 1988, AJ 96, 807
Tonry J.L., Schechter P.L., 1990, AJ 100, 1794
Tonry J.L., Ajhar E.A., Luppino G.A., 1990, AJ 100, 1416
Van den Bergh S., 1989, A&AR 1, 111
Willmer C.N.A., Focardi P., Nicolaci da Costa L., Pellegrini P.S., 1989, AJ 98, 1521
Wilson C.D., Freeman W.L., Madore B.F., 1990, AJ 99, 149
Zinn R., 1980, ApJS 42, 19